Article

Enhancement of Chiller Performance by Water Distribution on the Adiabatic Cooling Pad's Mesh Surface

Anatolijs Borodinecs ![ORCID], Kristina Lebedeva *, Natalja Sidenko and Aleksejs Prozuments ![ORCID]

Department of Heat Engineering and Technology, Riga Technical University, LV-1048 Riga, Latvia; anatolijs.borodinecs@rtu.lv (A.B.); natalja.sidenko@rtu.lv (N.S.); aleksejs.prozuments@rtu.lv (A.P.)
* Correspondence: kristina.lebedeva@rtu.lv

Abstract: Evaporative cooling is widely recognized as an energy efficient and environmentally-friendly air conditioning solution, and it has drawn a lot of market interest in recent years. However, this technology is accompanied by several challenges. For instance, insufficient evaporation due to poor and non-homogenous water distribution of the pre-cooling pad significantly reduces the cooling performance. The aim of the study is to develop a technique for numerical simulation of the distribution of a droplet liquid (water) on the mesh surface of an adiabatic cooler to improve the performance of air conditioning equipment. Modern computer-aided design (CAD)/computational fluid dynamics (CFD) programs were used to solve the issue. For the mathematical modelling of the medium motion, non-stationary Navier–Stokes equations were used. Parameters such as heat, mass transfer, and the efficiency of liquid droplet spraying were determined. The current study presents CAD modelling, conducted in SolidWorks platform, of water distribution on the adiabatic cooling pad's mesh surface for improving air conditioning equipment performance. This study provides the methodology for computer modeling and numerical calculation of the parameters of adiabatic cooling, such as modelling of water atomization process. The results show that the use of additional metal mesh intended as cooling pads increases the mass transfer coefficient by $Sh \approx 15$–40%; heat transfer coefficient Nu increases by ≈ 20–40%; and the atomization efficiency increases by ≈ 30–40%. The installation of metal pad mesh allows for equalized uniformity of the water distribution. The results imply that there are more opportunities to optimize the parameters of adiabatic cooling, which should be evaluated in further research on the subject.

Keywords: air conditioning; energy consumption; evaporative cooling; CAD/CFD; water atomization; cooling pad; energy saving

1. Introduction

Energy is one of the essential components of the development of human society. Rapid socio-economic developments and ever-increasing energy consumption have led to critical resource depletion and environmental pollution [1]. The world's population has grown, and this population growth rate has been faster in recent years; moreover, an individual demand for energy has increased as technological advancements continue [2]. As well as economic developments in emerging markets, the demand for energy services and technologies is expected to increase, including energy to ensure indoor comfort, safe food storage and preparation, communications, and entertainment industries, etc. [3]. Based on several recent studies [4,5], the number of electronic devices owned by each individual has increased substantially. As individual income levels and population are increasing, demand for air conditioning to improve the comfort of living spaces and offices is rising as well. Air conditioners and electric fans used to cool room temperatures account for almost 20% of all electricity consumed in buildings worldwide [6]. Rising energy consumption places a high load on electricity providers to meet peak demand [7]. Subsequently, there is an urgent need to find an energy efficient solution to this technology. Modern engineering systems

can be competitive only with maximum energy savings and a reduction in operating costs by using the most advanced technical solutions [8]. As a promising alternative, application of optimal water distribution pattern on the surface of direct adiabatic cooling pad's mesh surface is reviewed in this study.

The main structural elements of direct adiabatic coolers include a sprinkler—made in the form of mesh surfaces, various shapes, and materials; and water distribution system consisting of a pressurized tubular water distribution system and hydraulic centrifugal nozzles with a tangential supply. The system is designed for uniform distribution of cooled water over the surface of the sprinkler. As a result, the necessary surface of the water flow is created, which determines its cooling capacity, drop eliminator, and various other elements, depending on the type of cooler. The physical principle of the cooler is the process of heat and mass transfer through air–water surfaces. In a direct evaporative cycle, the air stream is cooled by direct contact with the liquid film and the cooling is carried out by interfacial heat exchange between the air stream and the liquid film. Evaporation of water in the air stream leads to a decrease in the temperature of the dry bulb. Meanwhile, at the same time, this leads to an increase in the humidity of the air flow.

Direct evaporative cooling is well known as an energy efficient air conditioning solution [9]. The use of an evaporative cooling approach can save energy, as cold water lowers the condenser temperature and may increase the rate of heat rejection [10,11]. In the recent study [12], the modeling results showed how the use of an evaporative cooler in a 200 m^2 residential house reduced the total energy consumption by 75% compared to traditional air conditioners. The cost of an evaporative cooling system for hot and dry climate regions is about 88% lower than that of a traditional conventional cooling system that uses electricity for cooling [13]. The results of the studies [14–16] showed an improvement in the performance of the entire air conditioning system—the cooling capacity improved from 5 to 18.6% using a direct evaporative cooling approach. In addition to the advantages described in the revised studies, the direct evaporative cooling system has its disadvantages, such as increased water consumption and the need of water preparation, as evaporation leaves the minerals in the air in the form of fine dust. For cooling towers this is a fairly inexpensive process involving coarse cleaning—cleaning is mainly provided to prevent scale formation—then the nozzles of the adiabatic system require microfilters and osmotic filtration. As a result, not only the system costs increase, but so do the operating costs. Although the price of water is not comparable to the cost of electricity, it is still constantly rising worldwide. Water consumption efficiency for cooling ranges from 0.45 MJ/L to 2 MJ/L [17]; it is obvious that older and cheaper adiabatic cooler models tend to use more water than the more recent and more advanced ones. Adiabatic cooler companies, as well as their end-users, need to consider water losses throughout the year, as they will be higher during the hot seasons. In the study [18], the water loss of an adiabatic cooler in summer is 5.2 L per hour. The report [19] examines about 100 published studies on evaporative cooling systems. The energy saving potential of the cooling process in this review was determined to range between 50–80% and systems effectiveness—between 80–110%. An extensive literature review indicates gaps in the research on the water atomization process and there is a significant need to develop improved water distribution systems that could enhance adiabatic cooling process performance. The authors also analyzed the available numerical studies on water mist technology in the adiabatic cooling process [20–22] and also identified the research gap in this field. As the wetting efficiency depends directly on the degree of water atomization, that is, on the size of the obtained droplets [23,24], the most optimal for evaporative cooling are spiral type nozzle [25], but the volume of sprayed water distribution is limited in many areas [26]. Another disadvantage of these nozzles is the non-homogeneity of the water distribution on the adiabatic cooling pad's mesh surface: the lower the water flow rate, the lower the surface wettability and cooling capacity [27]; as such, by increasing the wettability, the cooling performance was further improved [28]. Authors also note that many issues, due to the multifactorial nature of the ongoing processes, remain poorly understood. The process of spraying a liquid jet

is characterized by a complex physical phenomenon, which consists in crushing a liquid jet into a large number of drops and distributing these droplets in space; considering the ongoing processes of heat and mass transfer, it makes it practically impossible to use analytical methods and create a reliable theory. Full-scale tests are quite expensive and do not fully provide a complete picture of the ongoing complex physical phenomena. Known works using computational fluid dynamics (CFD) methods are mainly performed in a two-dimensional problem setting, and refer to specific special cases of problem solving. The purpose of this study is to develop a technique for numerical simulation of the distribution of a dropping liquid (water), taking into account heat and mass transfer on the mesh surface of an adiabatic cooler, to improve the performance of air conditioning equipment. To achieve this goal, modern methods of computational fluid dynamics (CAD/CFD) are used in a three-dimensional formulation of the problem. The mathematical description is based on non-stationary Navier–Stokes equations, taking into account heat transfer, which were solved numerically using the finite volume method. To find the desired numerical solution, a continuous non-stationary mathematical model of physical processes is discretized both in space and in time. Taking into account the complexity of the problem under consideration, for each considered diameter of the dropping liquid the following indicators were determined: velocity, viscosity, density, Reynolds criterion, which are included in the equations of heat and mass transfer coefficients, and spraying efficiency. Due to the limited experimental data, the grid convergence method was used to estimate the accuracy of the obtained solution.

The methods of numerical mathematical modelling used to determine the hydrodynamic heat and mass transfer parameters of an adiabatic cooler will provide information on the hydrodynamics of the sprayed liquid at the stage of development and verification of the model.

2. Materials and Methods

Within the framework of the project "Development of a new prototype of adiabatic cooling panels to ensure the sustainability and energy efficiency of cooling equipment", it was necessary to improve the cooling capacity and reduce the electricity consumption of air conditioning equipment. In our previous study [29], optimization of air conditioning equipment work was investigated by reducing the temperature of the inlet water for pre-cooling purposes for a direct evaporative cooling system, but this approach did not result in a significant effect on the cooling effectiveness [30,31]. Our research [32] investigates different cross-sectional metal pad mesh in adiabatic evaporative cooling pads according to their pre-cooling potential in comparison with currently available technological solutions.

The purpose of this research is to develop homogenous water distribution film on pre-cooling pad to improve chiller performance. Within the framework of this study, a CAD and experimental approach were carried out.

2.1. CAD Approach

The purpose of this study is formulation of the basic methodology of computer modelling and computation of parameters for an adiabatic cooling process. The methodology should provide the possibility of parametric computations, which adequately model the physical phenomena being studied and allow for determining the characteristics of interest to the practical application. In addition, the computations performed should correspond satisfactorily to the experimental data or known theoretical computations, confirming the adequacy of the developed methodology.

Currently, CAD systems are widely used in both modern enterprises and scientific research. The main goal of CAD is the ability to produce new products of better quality (quality, Q), at a lower cost (cost, C), and in a shorter amount of time (delivery, D). Therefore, the use of the huge memory capabilities of computers, their high processing speed, convenient graphical interface for automation of processes and linking the tasks of design with each other, experimentation, and manufacture are the pressing tasks right now. The use of

CAD reduces the time and cost of product development and release. CAD, computer-aided manufacturing (CAM), and computer-aided engineering (CAE) technologies are used for this purpose. This CAD/CAM/CAE software suite allows for resolution and performance of various tasks during product development and manufacturing at each stage of the product cycle [33–36].

Flow Simulation, built using CAD software SolidWorks and fully integrated into SolidWorks to compute fluid (gas or fluid) motion in 2D and 3D models, allows to investigate the heat exchange of these models through convection, radiation, and conductivity using the reliable computational fluid dynamics (CFD) technology. Flow Simulation features an intuitive and user-friendly interface, including a pre-processor for specifying data for computation (using an engineering database that contains information about the properties of substances), a coprocessor for monitoring and controlling computation, and a postprocessor for viewing the results obtained. Thus, it is possible to carry out various computations and to study and analyze the results obtained in detail [37].

In scope of this study, the practical validation of a development theoretical model was limited and is based on comparison with studies where SolidWorks was used. However, this does not neglect trust for theoretical analysis. The model is based on fundamental equations of conservation of momentum, mass, and energy describing turbulent, laminar, and transient flows of a compressible fluid with heat exchange. The next studies will be focused on practical measurement and comparison with theoretical outcomes. This paper could serve as input for the creation of a test chamber for any interested research group.

2.1.1. Physical Definition of the Problem

The computational physical model includes a simplified geometric design of water mist technology in the adiabatic cooling process, devoid of non-essential parts which have little influence on its physical characteristics.

Thus, the physical model under consideration can be endowed with only some of the properties of the real design. The simpler the geometric model is, the easier its mathematical description. The success of choosing the physical model of the design ultimately depends on the labor input of the computation and the accuracy of its results. Here, much depends on understanding the peculiarities of functioning of the design and the ability to distinguish only the characteristic parts that basically determine its performance.

The main design elements of adiabatic cooling equipment are nozzles spraying fluids on a special hard surface (pre-cooling pad), which can be made in the form of a metal mesh.

Using the SolidWorks parametric modeling program [37], a three-dimensional simplified geometric computer model of an adiabatic cooler was created. In the case under consideration, the adiabatic cooler model consists of two tangential nozzles, L-shaped pipeline, and pre-cooler pad (Figure 1). A three-dimensional model of a tangential nozzle of the TG 20 × 12 type was built according to known geometric parameters, with a diameter of the nozzle flow section d = 12 mm and a range of flow characteristics Q = 0.9–2.4 m^3/h or Q = 0.00025–0.000666 m^3/s. This type of nozzle is used to distribute water in coolers.

For numerical calculation, all parts are combined into one common assembly.

Two models were built: Model 1—without a metal pad mesh, and Model 2—with a metal pad mesh installed in front of the nozzles.

Figure 2 shows the schematic diagram of the adiabatic cooling process (model 2). The liquid (water) with the set volume flow rate Q (m^3/s) flows from pipeline 1 to mixing chamber 2 of the tangential nozzle, where the water is swirled and discharged through outlet port 3 (nozzle) into the airspace. When the liquid film comes out of the nozzle, it disintegrates, forming a single flare (jet) in the form of a cone and not limited by solid walls.

The nozzle is mounted at height H from the metal mesh with overall dimensions $a \times b \times h$ = 2000 mm × 1140 mm × 222 mm and square cells of 16 mm × 16 mm.
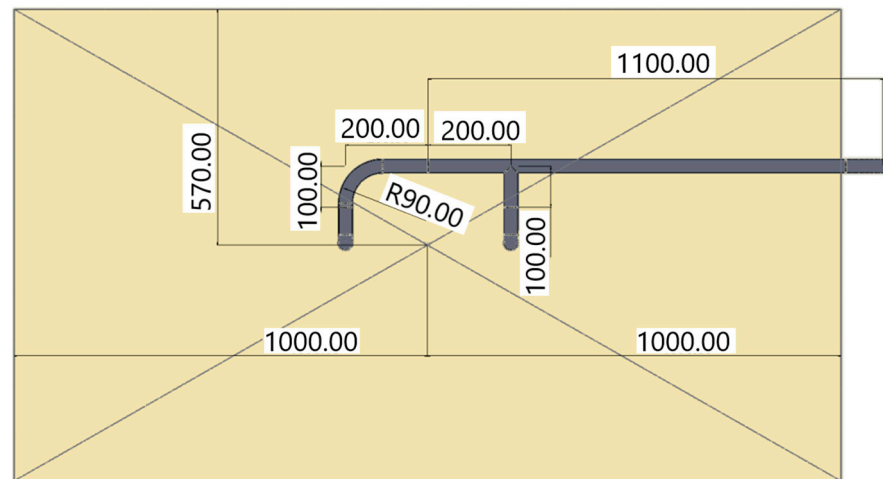
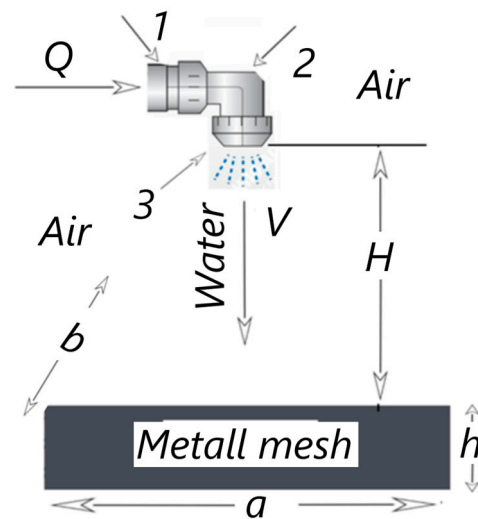**Figure 1.** Assembly drawing of an adiabatic cooler top view.

Figure 2. Diagram of the adiabatic cooling process.

Boundary conditions: For the numerical solution of the problem at the inlet to the L-shaped pipeline, the volumetric flow rate of water was set based on each nozzle: for case 1—Q = 0.00025 m³/s, for case 2—Q = 0.000666 m³/s. The ambient temperature (*air*) T_{AIR} and the temperature of the liquid (*water*) T_{WATER} entering the pipeline and then into the nozzles are equal to each other. T_{AIR} = T_{WATER} = 293.20 K (20 °C). Ambient pressure is equal to atmospheric p = 101325 Pa, density ρ = 1.2041 kg/m³, dynamic viscosity μ = 1.85 × 10⁻⁵ Pa·s, specific heat capacity at constant pressure Cp = 1005 J/(kg·deg).

Water: temperature T_{WATER} = 293.20 K (20 °C), density ρ = 998.16 kg/m³, dynamic viscosity μ = 0.0010014 Pa·s, specific heat capacity Cp = 4184.4 J/(kg·deg). The metal mesh is modelled as an isotropic porous body (the permeability of the medium is the same in all directions inside the medium). The effective porosity of the medium is determined by Equation (1), as the volume fraction of the pores connected together *Vpores* in the total volume of the porous medium *Vtotal*:

$$\varepsilon = \frac{V_{pores}}{V_{total}} \tag{1}$$

In the case under consideration, the porosity of the medium is ε = 0.5, and it is set by default.

The permeability of the medium к is determined by formula (2):

$$k = \frac{\Delta P}{V \cdot L \cdot \rho} \tag{2}$$

where ΔP—pressure difference between the opposite sides of the parallelepipedal porous body in the selected direction, Pa; V—flow rate of the fluid medium, m/s; ρ—fluid density, kg/m^3; L—length of the body in this direction, mm. The dependence of the pressure difference ΔP (Pa) on the flow rate of the liquid V (m/s) is shown in Figure 3.
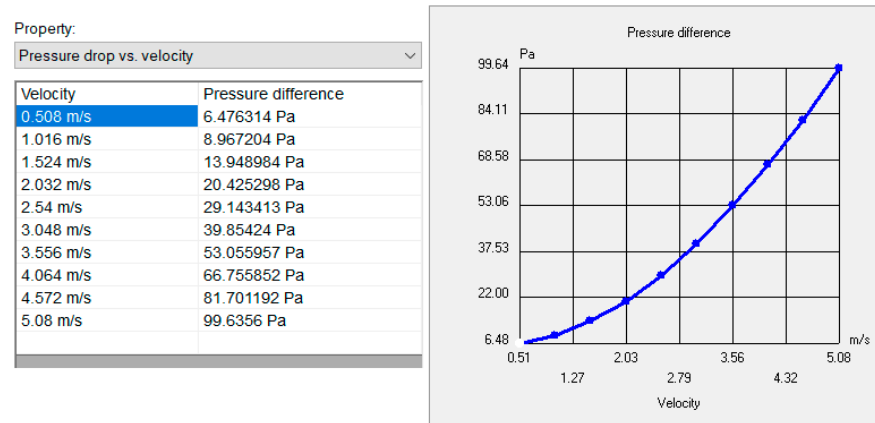

Figure 3. Dependence of pressure difference ΔP (Pa) on the flow rate of the liquid V (m/s).

For the 2nd model, an additional metal mesh in front of the nozzles is modeled as well as an isotropic porous body. The dependence of the pressure drop ΔP (Pa) on the fluid flow rate V (m/s), for the case under consideration, is shown in Figure 4.
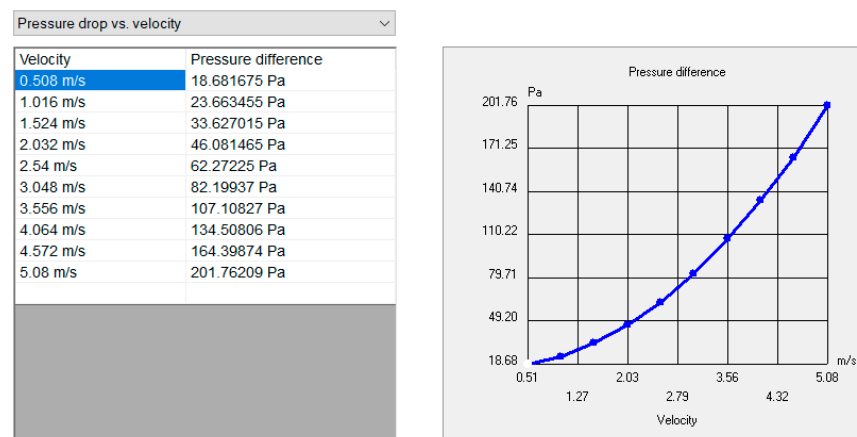

Figure 4. Dependence of pressure difference ΔP (Pa) on the flow rate of the liquid V (m/s).

The calculation of particle motion was considered in a steady flow of a fluid medium. The model of a fluid medium with liquid particles in Flow Simulation assumes spherical particles of constant mass, the effect of which on the flow is negligible, but the flow affects the speed and temperature (and hence the density) of the particles, which in turn affects their size.

For the particle calculation, the initial conditions were set: the entry points of the particles into the fluid medium (the outlet of the nozzle); the initial parameters of the particles: liquid-water, temperature $T_{partical}$ = 293.20 K (20 °C), density ρ = 998.16 kg/m^3, diameter-d = 100 µm and d = 500 µm, as well as the total mass flow (amount of particle mass, introduced by the fraction into the fluid per unit time) for the case of volume flow

$Q = 0.00025 \text{ m}^3/\text{s-mass flow } m = 0.249 \text{ kg/s, for } Q = 0.000666 \text{ m}^3/\text{s-}m = 0.6376 \text{ kg/s. In}$ particle motion calculation, gravity was taken into account, which was specified using the components of the gravitational acceleration vector in the global coordinate system.

2.1.2. Mathematical Formulation of the Problem

The non-steady-state Navier–Stokes equations, the energy equation (first law of thermodynamics), and the equation of [38–41] are used for mathematical modelling of the motion of the medium. For turbulent flows, the initial equations of Reynolds-averaged and additional stresses due to turbulent pulsations of parameters are taken into account [37]. The obtained non-closed system of equations is closed by means of additional equations for kinetic energy of turbulence k and dispersion of energy of turbulence ε in accordance with the known *k-ε* turbulence model [42].

The system of equations of conservation of momentum, mass, and energy describing turbulent, laminar, and transient flows of a compressible fluid with heat exchange can be represented as:

$$\frac{\partial \rho u_i}{\partial t} + \frac{\partial}{\partial \chi_j}\left(\rho u_i u_j - \tau_{ij}\right) + \frac{\partial P}{\partial \chi_i} = F_i, \tag{3}$$

$$\frac{\partial \rho}{\partial t} + \frac{\partial}{\partial \chi_j}\left(\rho u_j\right) = 0, \tag{4}$$

$$\frac{\partial(\rho E)}{\partial T} + \frac{\partial}{\partial \chi_i}\left((\rho E + P)u_i + q_i - \tau_{ij}\, u_j\right) = F_i u_i + Q_H, \tag{5}$$

$$\frac{\partial \rho k}{\partial t} + \frac{\partial}{\partial \chi_i}\left(\rho u_i k\right) = \frac{\partial}{\partial \chi_i}\left(\left(\mu_l + \frac{\mu_t}{\sigma_k}\right)\frac{\partial k}{\partial \chi_i}\right) + S_k, \tag{6}$$

$$\frac{\partial \rho \varepsilon}{\partial t} + \frac{\partial}{\partial \chi_i}\left(\rho u_i \varepsilon\right) = \frac{\partial}{\partial \chi_i}\left(\left(\mu_l + \frac{\mu_t}{\sigma_\tau}\right)\frac{\partial \varepsilon}{\partial \chi_i}\right) + S_\tau, \tag{7}$$

$$S_k = \tau_{ij}^R \frac{\partial u_i}{\partial \chi_j} - \rho\varepsilon + \mu_t P_B; \; \rho = \frac{P}{RT}; \; q_i = -\left(\frac{\mu_l}{P_r} + \frac{\mu_t}{\sigma_c}\right)c_P\frac{\partial T}{\partial \chi_i}, \tag{8}$$

$$S_\varepsilon = C_{\varepsilon 1}\frac{\varepsilon}{k}\left(f_1\tau_{ij}^R\frac{\partial u_i}{\partial \chi_j} + \mu_t C_B P_B\right) - C_{\varepsilon 2}f_2\frac{\rho\varepsilon^2}{k}; \; P_B = -\frac{g_i}{\sigma_B}\frac{1}{\rho}\frac{\partial\rho}{\partial \chi_i}, \tag{9}$$

$$\tau_{ij} = (\mu_l + \mu_t)\left(\frac{\partial u_i}{\partial \chi_i} + \frac{\partial u_j}{\partial \chi_i} - \frac{2}{3}\frac{\partial u_l}{\partial \chi_l}\delta_{ij}\right) - \frac{2}{3}\rho k\delta_{ij};$$
$$f_1 = 1 + \left(\frac{0.05}{f_\mu}\right)^3; \; f_2 = 1 - exp\left(-\left(\frac{\rho k^2}{\mu_l \varepsilon}\right)^2\right), \tag{10}$$

$$\tau_{ij}^R = \mu_t\left(\frac{\partial u_i}{\partial \chi_i} + \frac{\partial u_j}{\partial \chi_i} - \frac{2}{3}\frac{\partial u_l}{\partial \chi_l}\delta_{ij}\right) - \frac{2}{3}\rho k\delta_{ij}, \tag{11}$$

$$\mu_t = f_\mu\frac{C_\mu\rho k^2}{\varepsilon}; \; f_\mu = [1 - exp(-0.025\frac{\rho\sqrt{k}y}{\mu_l})]^2\cdot(1 + \frac{20.5\,\mu_l\varepsilon}{\rho k^2}), \tag{12}$$

where *u*, *p*, *ρ*, *T*—velocity, pressure, density, and temperature of the fluid, *R*—gas constant, *t*—time, *Fi*—total force acting on a unit of mass, *E*—total energy of the unit of mass of the fluid, Q_H—source of heat per unit volume, q_i—diffusion flow of heat, δij—Kronecker symbol, τ_{ij}—tensor of viscous shearing stresses, $\tau_{ij}^R \equiv -\rho u_i u_j$—stress tensor in the Reynolds model, μL—dynamic coefficient of viscosity, μ_t—coefficient of turbulent viscosity, *y*—distance from the solid wall, g_i—components of gravitational acceleration in the direction of x_i; σ_c, σ_B, σ_k, σ_ε, C_B, C_μ, $C_{\varepsilon 1}$, $C_{\varepsilon 2}$—empirical constants; *Cp*—specific heat capacity at constant pressure; *λ*—coefficient of thermal conductivity of gas (fluid); *Pr* = *μcp*/*λ*—Prandtl number; for laminar flow the parameters *k*, μ_t, *ε*—are equal to zero; *x*, *y*, *z*—current coordinates; summing takes place using the suffix numbers *i*, *j* = *x*, *y*, *z*.

This paper used the Flow Simulation CAE engineering software, in which the Navier–Stokes equations were solved numerically using the finite volume method.

Before starting the calculation, an approximation of the surfaces of solids (nozzles and metal mesh) in contact with the fluid medium is made, and for this the procedure of local fragmentation of the mesh cell near these areas of surfaces is used. So, each cell of the base mesh, intersected by the surface of a solid at the interface with a fluid medium, is divided into eight identical, geometrically similar cells of a smaller size. The discrete solution of the formulated continuous (differential) mathematical problem obtained on the computational grid formed in this way generally depends on the size of the computational grid cells that cover the computational domain. To solve the given mathematical problem and estimate the achieved accuracy, several calculations were carried out on different, rarer, and more frequent computational grids. To achieve a satisfactory accuracy of solving a mathematical problem (grid convergence), it took about 400,000 elements.

2.1.3. Methods for Processing the Results of Numerical Calculations

Authors studied liquid drops with diameters d = 100 μm and d = 500 μm, which are formed during the decay of the jet flowing from nozzles *f1* (right nozzle) and *f2* (left nozzle) (Figure 1).

For each diameter of the droplet liquid, the following indicators were determined: velocity, viscosity, density, Reynolds criterion, which are included in the equations of heat and mass transfer coefficients (13), (14), as well as the efficiency of atomization (15) [43,44]. Data were taken along the trajectory of liquid droplets from the nozzle outlet to the adiabatic cooler. Currently, quite a lot of criterion equations are known for determining the coefficients of heat and mass transfer depending on the physicochemical properties and regime parameters obtained on the basis of experimental data [44]. In this work, criterial equations were chosen: for the mass transfer coefficient *Sh*—the Kinzer equation (13), for the heat transfer *Nu*—the Lyakhovsky equation (14). These equations are characterized by the fact that, regardless of the experimental conditions, the nature and physical properties of the liquid, these equations provide relatively accurate results in a wide range of the Reynolds criterion *Re*.

The mass transfer coefficient *Sh*, was determined according to Equation (13):

$$Sh = 2 + 0.6Re^{0.5} \cdot Sc^{0.33}, \tag{13}$$

where *Re*—Reynolds number; *Sc*—Schmidt number.

The heat transfer coefficient *Nu*, Equation (14):

$$Nu = 0.62 \cdot Re^{0.5}, \tag{14}$$

Atomization efficiency η, Equation (15):

$$\eta = \frac{12\sigma}{d \cdot \rho \cdot w^2}, \tag{15}$$

where σ is the coefficient of surface tension of a liquid drop; d—droplet diameter (m); ρ—liquid density (kg/m^3); w—the speed of droplet movement (m/s).

The calculation of particle motion allows obtaining visualized images how liquid particles with mass (droplet) are distributed in the flow.

3. Results and Discussion

The results of the numerical calculation showed (visualization of the pattern of the distribution of liquid drops in Figure 5) that a finer spray of liquid droplets d = 100 μm (Figure 5 blue drops) is closer to the jet axis. Drops of larger diameter d = 500 μm (red color drops) are concentrated at the periphery of the jet. The data obtained are consistent with the known literature data [43,44].
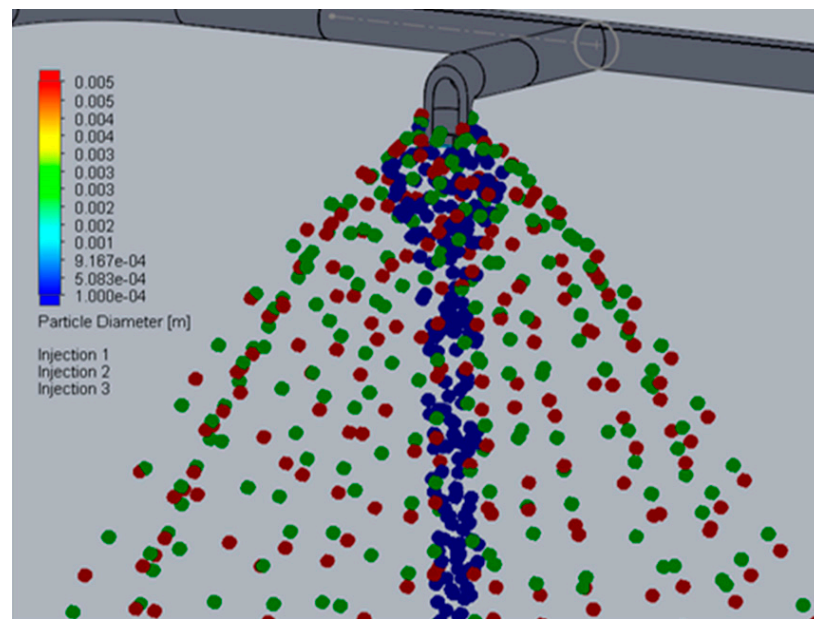
Figure 5. Visualizing the distribution pattern of liquid droplets.

Figure 6a,b shows the results of a numerical calculation of the mass transfer coefficient *Sh* relative to the trajectory of the particle from the nozzle outlet (*f1*—right nozzle, *f2*—left nozzle) to the pre-cooler pad. For cases $Q = 0.00025$ m^3/s (Figure 6a), and $Q = 0.000666$ m^3/s (Figure 6b) with and without installed metal pad mesh in front of the nozzle. Liquid particle diameter $d = 500$ μm Figure 6a,b. Liquid particle diameter $d = 100$ μm Figure 7a,b.
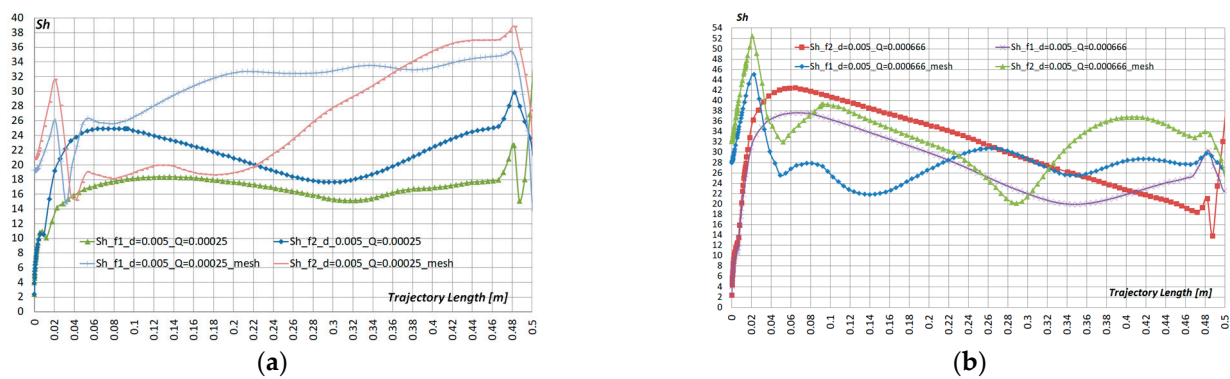
Figure 6. Mass transfer coefficient *Sh*, $d = 500$ μm: (**a**) $Q = 0.00025$ m^3/s; (**b**) $Q = 0.000666$ m^3/s.
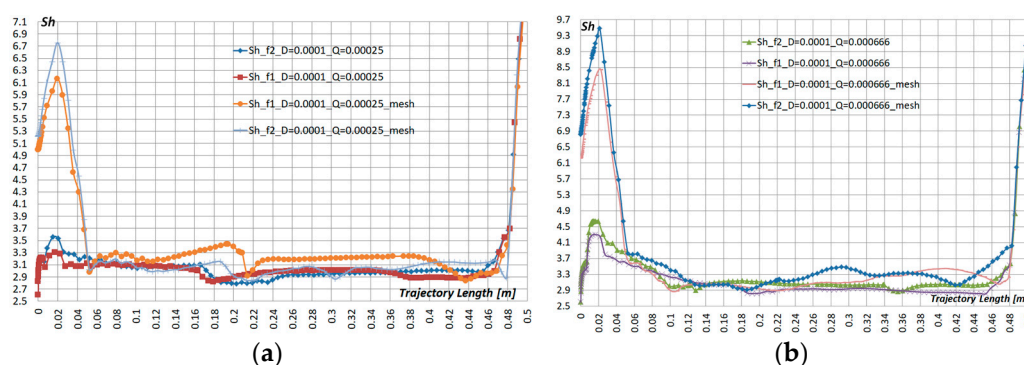
Figure 7. Mass transfer coefficient *Sh*, $d = 100$ μm: (**a**) $Q = 0.00025$ m^3/s; (**b**) $Q = 0.000666$ m^3/s.

The average values of the mass transfer coefficient *Sh* are summarized in Table 1.

Table 1. The average values of the mass transfer coefficient *Sh*.

	Q = 0.00025	Sh	Q = 0.000666	Sh
d = 0.0001	*f1*	3.311782	*f1*	3.509563
	f2	3.320845	*f2*	3.676473
	f1 mesh	3.942006	*f1* mesh	4.540239
	f2 mesh	3.943016	*f2* mesh	4.930458
d = 0.005	*f1*	16.11704	*f1*	24.17137
	f2	19.87923	*f2*	27.27551
	f1 mesh	28.44891	*f1* mesh	28.66047
	f2 mesh	25.21438	*f2* mesh	34.43927

The obtained results show that for the particle diameter d =100 µm and Q = 0.00025 m^3/s, a low mass transfer coefficient *Sh* is typical for both the first and second nozzles. However, the installed metal pad mesh increases the *Sh* coefficient for both nozzles by ≈15%.

For particle diameter d = 500 µm and Q = 0.00025 m^3/s, compared to particles d = 100 µm, there is a noticeable increase in the coefficient *Sh* ≈ by 70–80%. At the same time, with a metal pad mesh for d = 500 µm, *Sh* increases by 20–40%.

A similar pattern was also observed at Q = 0.000666 m^3/s, for particles d = 500 µm and d = 100 µm, compared with Q = 0.00025 m$_3$/s. The *Sh* coefficient increases, and the installed metal pad mesh increases *Sh* ≈ up to 30%.

Such changes in the *Sh* coefficient are due to two main parameters: the kinematic viscosity of the liquid, and the Reynolds number of a liquid drop, which are included in Equation (13). At the same time, for liquid drops d = 500 µm compared to d = 100 µm, the Reynolds number increases by ≈40–60%, and the kinematic viscosity of the liquid by ≈2–16%.

Figure 8a,b shows the results of a numerical calculation of the heat transfer coefficient *Nu* relative to the trajectory of the particle from the nozzle outlet (*f1*—right nozzle, *f2*—left nozzle) to the pre-cooler pad. For cases Q = 0.00025 m^3/s (Figure 9a), and Q = 0.000666 m^3/s (Figure 9b) with and without installed metal pad mesh in front of the nozzle. Liquid particle diameter d = 500 µm Figure 8a,b. Liquid particle diameter d = 100 µm Figure 9a,b.
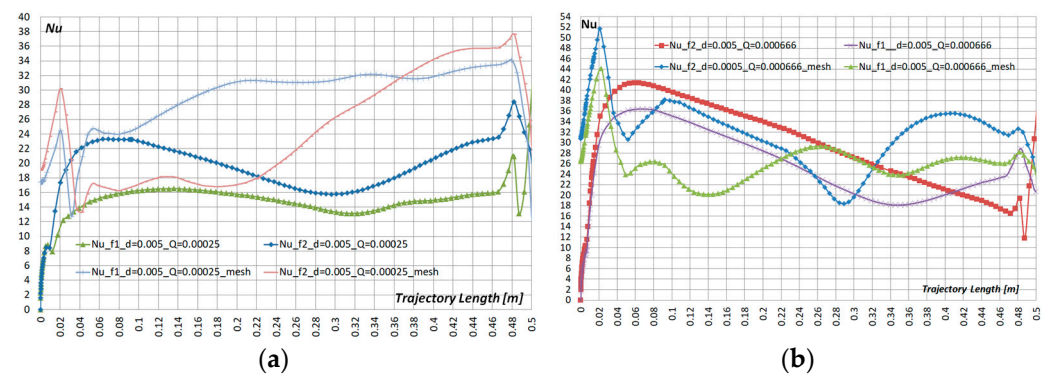

Figure 8. Heat transfer coefficient *Nu*, d = 500 µm: (**a**) Q = 0.00025 m^3/s; (**b**) Q = 0.000666 m^3/s.
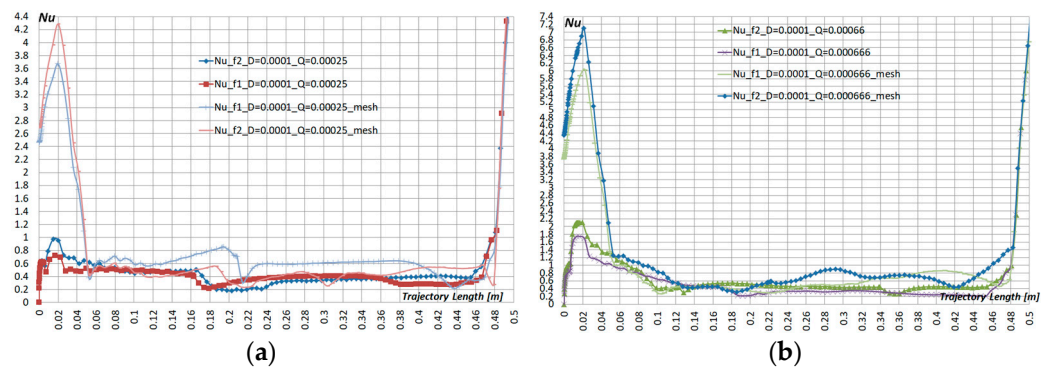
Figure 9. Heat transfer coefficient Nu, $d = 100$ µm: (**a**) $Q = 0.00025$ m^3/s; (**b**) $Q = 0.000666$ m^3/s.

The average values of the heat transfer coefficient Nu are summarized in Table 2.

Table 2. The average values of the heat transfer coefficient Nu.

	$Q = 0.00025$	Nu	$Q = 0.000666$	Nu
$d = 0.0001$	$f1$	0.719422	$f1$	0.927462
	$f2$	0.728958	$f2$	1.099443
	$f1$ mesh	1.369552	$f1$ mesh	1.992825
	$f2$ mesh	1.372388	$f2$ mesh	2.396427
$d = 0.005$	$f1$	14.17148	$f1$	22.49213
	$f2$	18.05553	$f2$	25.70276
	$f1$ mesh	26.90797	$f1$ mesh	27.19304
	$f2$ mesh	23.56767	$f2$ mesh	33.09933

The obtained results show that for particle diameters $d = 100$ µm and $Q = 0.00025$ m^3/s, $Q = 0.000666$ m^3/s, a low heat transfer coefficient Nu is relevant for both the first and second nozzles. At $d = 500$ µm and the same liquid flow rates, the heat transfer coefficient Nu increases significantly compared to particles $d = 100$ µm and can reach 90%. It is connected with the increase in the Reynolds number included in Equation (14).

Figures 10 and 11 show the results of the atomization efficiency η. It has to be noted that, according to the known data [43,44], the energy used on the formation of a new surface is not substantial—the efficiency of spraying usually does not exceed hundredths of a percent (the highest efficiency for hydraulic nozzles is about 0.04%)—and depends primarily on the physical properties of the liquid. Average atomization efficiencies are summarized in Table 3.
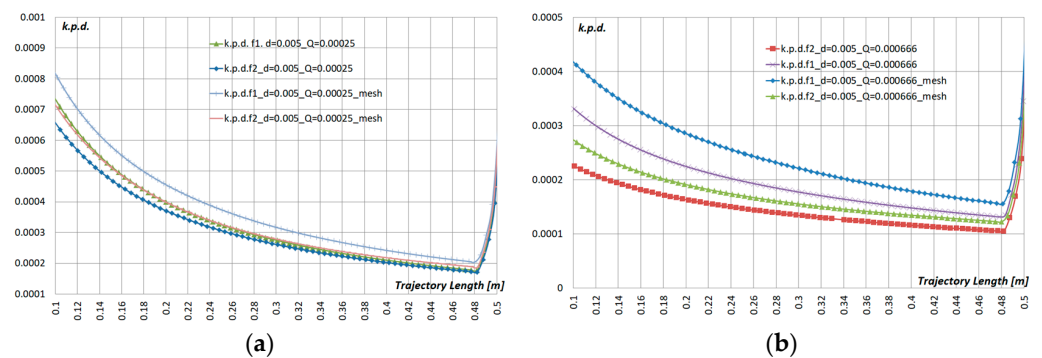

Figure 10. Atomization efficiency η, $d = 500$ µm: (**a**) $Q = 0.00025$ m^3/s; (**b**) $Q = 0.000666$ m^3/s.
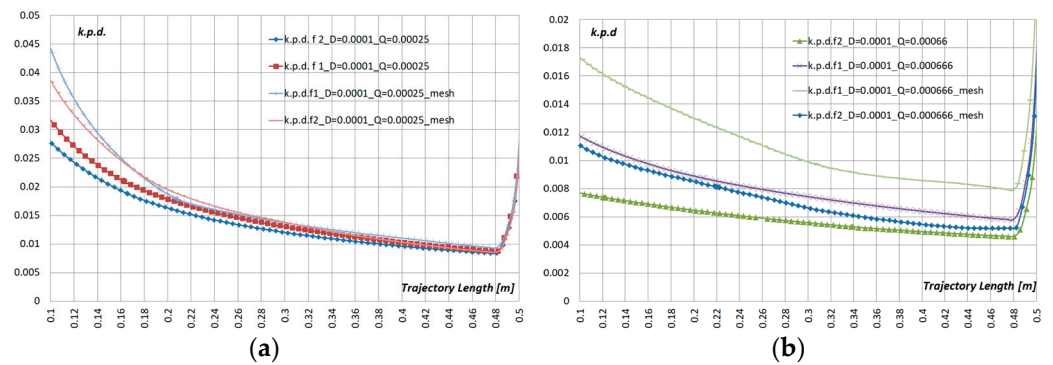
Figure 11. Atomization efficiency η, $d = 100$ μm: (**a**) $Q = 0.00025$ m^3/s; (**b**) $Q = 0.000666$ m^3/s.

Table 3. The average atomization efficiencies η.

	$Q = 0.00025$	η	$Q = 0.000666$	η
$d = 0.0001$	f1	0.054693	f1	0.016712
	f2	0.037475	f2	0.010037
	f1 mesh	0.020881	f1 mesh	0.04781
	f2 mesh	0.023857	f2 mesh	0.031201
$d = 0.005$	f1	0.054693	f1	0.000359
	f2	0.000796	f2	0.00024
	f1 mesh	0.002619	f1 mesh	0.000906
	f2 mesh	0.001852	f2 mesh	0.000664

The atomization efficiency is not uniform, and the highest efficiency is observed at liquid flow rate $Q = 0.00025$ m^3/s and d =100 μm, $d = 500$ μm, at the first nozzle $\eta = 0.054$. However, the installed metal pad mesh, in all other cases, improves the efficiency value by $\approx$30–40%.

During the disintegration of the jet, the interaction of forces of various nature on the surface of the liquid disrupts its integrity and crushing occurs. These forces include the forces of inertia, surface tension, aerodynamic forces, and viscous friction forces. To estimate the relationship between the forces in this work, the characteristic Reynolds numbers Re (14), Weber We (16) were used [43].

$$We = \frac{d \cdot \rho \cdot w^2}{\sigma}, \tag{16}$$

where w—the speed of droplet movement (m/s); d—the particle diameter (m); ρ—the density of the liquid (kg/m^3); σ—the force of the surface tension of the liquid (N/m).

The analysis of the obtained results showed, for example, for the case of a given calculated volumetric flow rate $Q = 0.0006$ m^3/s, the value of the average value of the criterion $Re_{d=500}$ along the trajectory of the liquid particle for $d = 500$ μm is much higher than its value, compared to $Re_{d=100}$ for particles d = 100 μm. That is, $Re_{d=500} > Re_{d=100}$ or $Re_{d=500} = 1560 > Re_{d=100} = 9.45$. A similar picture is also observed for the Weber test: $We_{d=500} > We_{d=100}$ or $We_{d=500} = 486 > We_{d=100} = 11.58$.

Calculations taking into account the additional installed mesh and without it, showed that the criterion $Re(mesh)_{d=100}$ for $d = 100$ μm almost doubles $Re(mesh)_{d=100} > Re_{d=100}$, $Re(mesh)_{d=100} = 22.76 > Re_{d=100} = 9.45$. For d = 500 μm, 1.2 times $Re(mesh)_{d=500} > Re_{d=500}$, $Re(mesh)_{d=500} = 1967 > Re_{d=500} = 1560$. In this case, the criterion We decreases, and for $d = 100$ μm is $We(mesh)_{d=100} = 7.9$, i.e., tends to the minimum value $We_{Kp} = 7$. Presumably, passing through the additional mesh (obstacle) the velocity of liquid particles decelerates and breaks up. The average droplet velocity at a distance from the nozzle outlet to the exit from the additional mesh is two times less than in the calculations without the mesh $w(mesh) < w$, $w(mesh) = 0.85$ m/s $< w = 1.6$ m/s.

For d = 500 μm, *We(mesh)* $_{d = 500}$ = 386 < *We* $_{d = 500}$ = 486, taking into account that the criterion *We (mesh)* is in the range 10 < We < 104, then the form of droplet destruction occurs in the same way, as in the case considered above, for d = 500 μm, *We d = 500*.

Based on the above, it can be assumed that a significant influence on the value of the heat and mass transfer criteria, as well as on the efficiency, is influenced by the diameter of the liquid droplets, their physical properties, as well as additional forces affecting the flow of the dropping liquid.

Figure 12 shows the pattern of liquid particle atomization formation at the initial moment of time, that is, when the flow of the supplied liquid in the pipeline with a given volumetric flow rate has not yet been established. It can be seen that in the right nozzle (*f1*), the torch (jet) is already fully formed, and in the left nozzle (*f2*) it is just beginning to form. At the same time, spraying of a finer fraction of a particle with a diameter of d =100 μm (blue particles) is already observed at both nozzles and is closer to the axis of the torch (jet). The spray of larger particles with a diameter of d = 300 μm (green particles) and d = 500 μm (red particles) at the right nozzle is already fully formed, at the left nozzle in the inlet section, these particles are just beginning to form. Such non-uniformity of the spray may be due to the fact that when the liquid moves through the distribution pipeline on which the nozzles are installed, there is a gradual decrease in the flow rate and velocity of the liquid in the pipe.
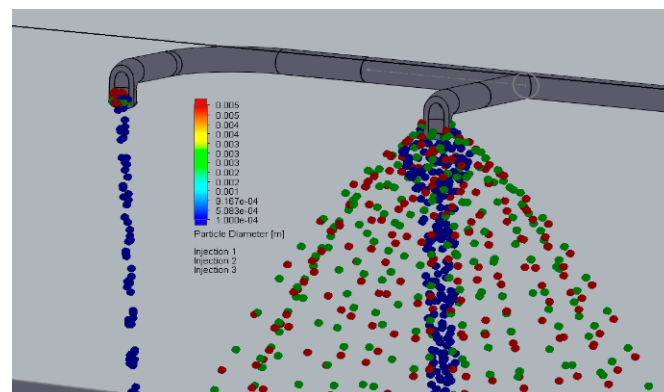

Figure 12. The pattern of liquid particle atomization formation.

In Figure 13 the distribution patterns of the liquid flow rate for a given volumetric flow rate Q = 0.00025 m^3/s are presented: (**a**) without metal pad mesh and (**b**) with metal pad mesh. The figures show that the installation of the metal pad mesh somewhat narrows the liquid jet, but at the same time, when it reaches the pre-cooler pad, it reduces the intensity of vortex formation and the liquid flow passes through the pad mesh more evenly.

Figure 13 shows the distribution patterns of the liquid flow rate for the volumetric flow rate Q = 0.000666 m^3/s: (c) without metal pad mesh and (d) with metal pad mesh. In the case with a lower flow rate, for the scenario with metal pad mesh, there is noticeably less intense vortex formation above the pre-cooler pad. It is also observed that there is less obvious compression of the jet and a more uniform distribution of the fluid flow velocity, when passing through the metal mesh.

Figure 14 shows the distribution of mass concentration of water in the calculated volume filled with air (front view) for water flow Q = 0.00025 m^3/s and for Q = 0.000666 m^3/s: (c) without metal pad mesh and (d) with metal pad mesh. The figure shows that the mass concentration of water is more evenly distributed in the adiabatic cooler for the case with the installed metal pad mesh. Presumably, such a distribution is achieved by less intense vortex formation above the pre-cooler.
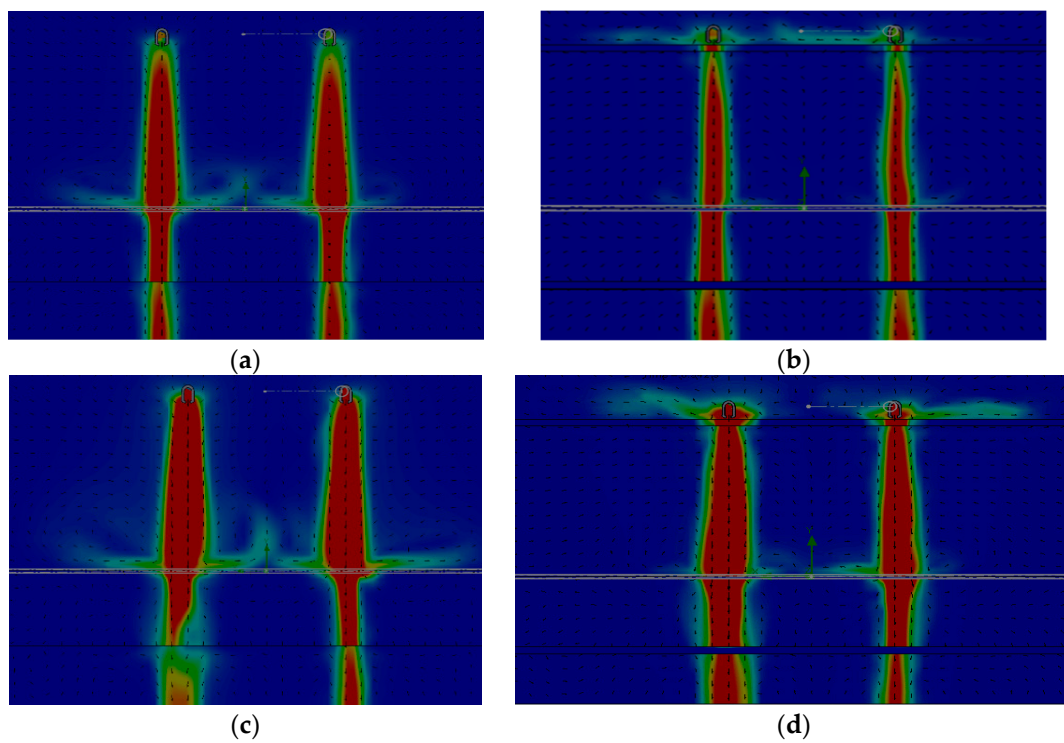
Figure 13. Fluid flow rate distribution patterns for: $Q = 0.00025$ m^3/s: (**a**) without metal pad mesh and (**b**) with metal pad mesh; $Q = 0.000666$ m^3/s: (**c**) without metal pad mesh and (**d**) with metal pad mesh.
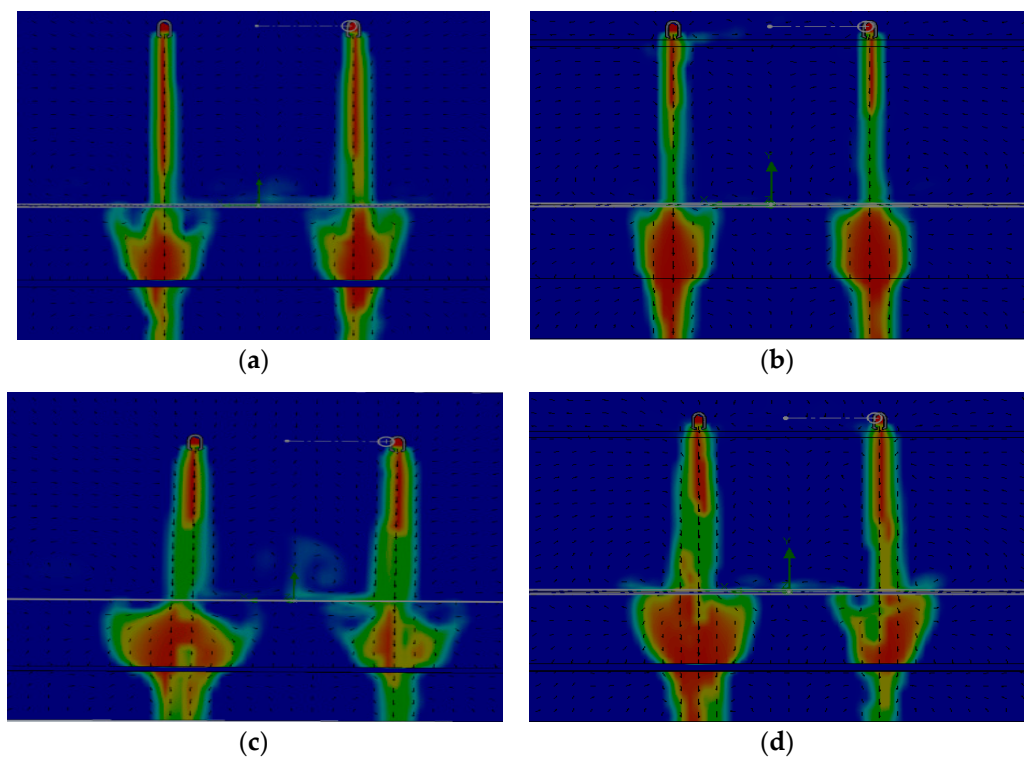

Figure 14. The distribution of mass concentration of water for: $Q = 0.00025$ m^3/s: (**a**) without metal pad mesh and (**b**) with metal pad mesh; $Q = 0.000666$ m^3/s: (**c**) without metal pad mesh and (**d**) with metal pad mesh.

To assess the accuracy of solving the problem, a free jet was considered, created by a single tangential nozzle of the TG 20 × 12 type, moving in space in the absence of side walls. A three-dimensional model of the nozzle was built according to the geometric dimensions presented in the datasheet. Nozzle flow characteristics in the range $Q = 0.9 \text{ m}^3/\text{h} - 2.4 \text{ m}^3/\text{h}$. Working pressure $p = 29.42–343$ kPa.

During the calculation, the jet opening angle, the distribution of liquid droplets in a jet with a given diameter, density, viscosity, velocities, and pressure required for calculation of the Reynolds and Weber numbers were determined.

Comparative analysis of calculation results with theoretical studies [44] showed:

— The theoretical jet opening angle was calculated according to the well-known method described in [44]. The obtained numerical solution well matched with the results of the theoretical calculation of the jet, and the error does not exceed 10%. Jet opening angle (theoretical) $\varphi_{teoret} = 20°$, numerical calculation $\varphi_{nc} = 22°$. Figure 15 shows visualization of the distribution of a steady liquid jet for a volumetric flow rate $Q = 0.00025 \text{ m}^3/\text{s}$: (a) numerical calculation (visualization is presented in the form of a dropping liquid), (b) experiment. Figure 15a shows that the shape of the outflowing jet, at the outlet of the nozzle, has a small section of a cylindrical shape, and further downstream the jet opens up, taking a full cone-shaped shape. A similar flow was observed in the experiment (see Figure 15b).

— The speed of the drops w along the trajectory are not uniform and as the jet breaks up it is $w = 0.5–3$ m/sec. Drops of a smaller diameter $d = 100$ mkm create a cylindrical jet, at $d = 500$ mkm a conical jet, in the general case, creating a full-cone jet. The result of the calculation is well matched with the manufacturer experimental visualized data of the considered type of nozzle.
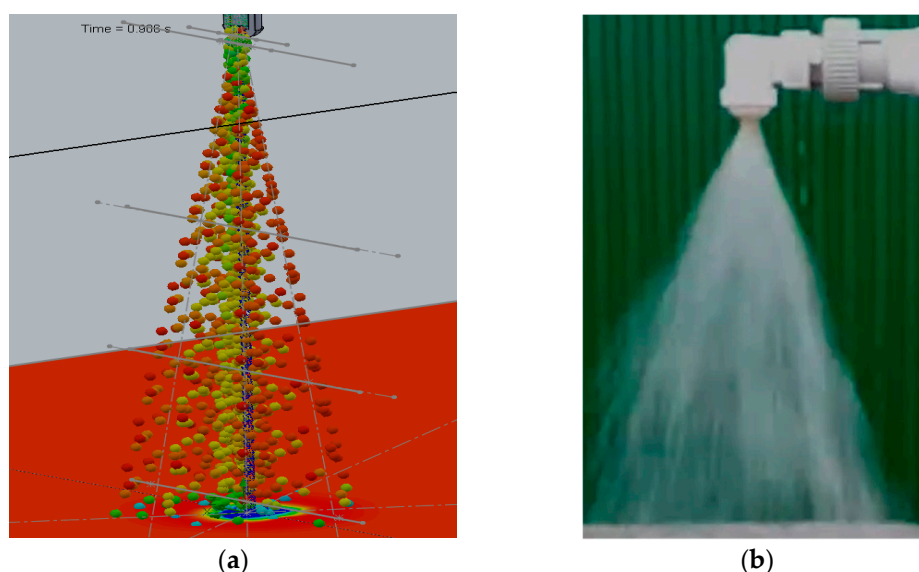

| (a) | (b) |

Figure 15. Visualization of the distribution of a steady liquid jet for a volume flow $Q = 0.00025 \text{ m}^3/\text{s}$. (**a**) Numerical calculation, (**b**) experiment.

At a volumetric flow rate of liquid $Q = 0.9 \text{ m}^3/\text{h}$, there are two zones of disintegration of liquid droplets: in the first zone 1 Weber criterion $0.1 \leq We \cdot Re^{-0.5} \leq 0.8$ (zone 1), division into 2–4 drops occur, the "bag" is destroyed and chaotic fragmentation; in the second zone $0.8 \leq We \cdot Re^{-0.5} \leq 10$, droplets are destroyed with a breakdown of the surface layer, giving a very fine spray along with large secondary particles separated from the original drop. In this case the calculated working pressure is in the range $p = 102.32–104.82$ kPa; it does not exceed the working pressure, according to the manufacturer datasheet of the nozzle.

All of the above-studied cases, as well as this research, are dedicated to improving the efficiency of evaporative air conditioning equipment. In the study [32], experiments were

carried out under laboratory conditions (Figure 16) to identify the pre-cooling potential of various types of metal mesh intended as cooling pads of various shapes (W, Z, Z1) with square cells of 16 × 16 mm (Figure 17). In the presented case, a straight metal mesh was modeled (a flat, non-curved metal pad mesh). In the future, it is planned to create models in SolidWorks for various metal mesh shapes (W, Z, Z1) and validate the model with real measurements. The created models will help to quickly and efficiently select the required sizes and shapes of pre-cooling pads, as well as to optimize the water/air supply, thereby increasing the efficiency of evaporative air conditioning equipment.

Figure 16. Testing setup in laboratory conditions.

Figure 17. Example of different testing metal mesh.

The previous study on this subject [29] show that the environmental benefit of the evaporative cooling system is superior to that of the conventional system with annual electricity saving potential in the ballpark of 45–50% which consequently reduces CO_2 emissions produced by power plants. Increasing the area of the pre-cooler pad, by using the metal mesh intended as cooling pads of various shapes, will significantly reduce fossil fuel consumption during peak loads. The distribution of water on the adiabatic cooling pad's mesh surface also plays an important role in the performance of an evaporative cooler. In addition, precise control of water atomization helps to reduce the environmental impact of cooling processes by reducing water consumption.

4. Conclusions

The main conclusions are summarized below:

1. It was revealed in the considered design cases, that when the liquid is supplied through the pipeline to the nozzles from one side in the presented design they do not work evenly.
2. Assessment of the accuracy of the problem under consideration showed agreement with the results of theoretical studies and manufacturer experimental visualized data.
3. The results of calculating the mass transfer coefficient showed that for particles $d = 100$ μm, $Q = 0.00025$ m³/s, and $Q = 0.000666$ m³/s, a relatively low mass transfer

coefficient $Sh \approx 3.3$–3.5 is typical. The installation of metal pad mesh allowed to increase $Sh \approx 15\%$. For particles $d = 500$ μm, compared to particles $d = 100$ μm, the Sh coefficient increased by 70–80%, and the additional metal mesh increased Sh factor by another 20–40%.

4. Heat transfer coefficient Nu for $d = 500$ μm compared to particles $d = 100$ μm increased by 90% and the additional metal mesh increased Nu by another 20–40%.

5. The atomization efficiency has its own value for each nozzle and the highest atomization efficiency was observed at liquid flow rate $Q = 0.00025$ m^3/s and $d = 100$ μm, $d = 500$ μm. An additional metal pad mesh, in all other cases considered, improved the efficiency value by $\approx$30–40%.

6. Visualization patterns of the fluid flow rate showed that at the jet periphery, upon impact with an adiabatic pre-cooler pad, return flows were formed, which, presumably, affected the uniformity of the liquid mass concentration in the pre-cooler itself. The installation of an additional metal pad mesh makes it possible to reduce vortex formation above the pre-cooler pad and, as a result, to equalize the uniformity of the distribution of the mass concentration of the liquid.

7. Processing the simulation results, it was found that the use of metal pad mesh promotes the smoothest and most uniform water distribution of pre-cooling pad that improves environmental benefit by increasing efficiency values by $\approx$20–40% and reducing the water consumption of the system by $\approx$15–20%.

References

1. Xue, J.; Ding, J.; Zhao, L.; Zhu, D.; Li, L. An option pricing model based on a renewable energy price index. *Energy* **2022**, *239*, 122117. [CrossRef]
2. Sen, D.; Tunç, K.M.; Günay, M.E. Forecasting electricity consumption of OECD countries: A global machine learning modeling approach. *Util. Policy* **2021**, *70*, 101222. [CrossRef]
3. Waite, M.; Cohen, E.; Torbey, H.; Piccirilli, M.; Tian, Y.; Modi, V. Global trends in urban electricity demands for cooling and heating. *Energy* **2017**, *127*, 786–802. [CrossRef]
4. Hischier, R.; Böni, H.W. Combining environmental and economic factors to evaluate the reuse of electrical and electronic equipment–a Swiss case study. *Resour. Conserv. Recycl.* **2020**, *166*, 105307. [CrossRef]
5. Mir, A.; Alghassab, M.; Ullah, K.; Khan, Z.; Lu, Y.; Imran, M. A Review of Electricity Demand Forecasting in Low and Middle Income Countries: The Demand Determinants and Horizons. *Sustainability* **2020**, *12*, 5931. [CrossRef]
6. International Energy Agency's (IEA). *The Future of Cooling Opportunities for Energyefficient Air Conditionin*; IEA: Paris, France, 2018.
7. Alawadhi, M.; Phelan, P.E. Review of Residential Air Conditioning Systems Operating under High Ambient Temperatures. *Energies* **2022**, *15*, 2880. [CrossRef]
8. Titova, E.M.; Averyanova, O.V. Efficiency evaluating of air conditioning system with air dehumidification section. *Mag. Civ. Eng.* **2011**, *19*, 46–52. [CrossRef]
9. Tejero-González, A.; Franco-Salas, A. Optimal operation of evaporative cooling pads: A review. *Renew. Sustain. Energy Rev.* **2021**, *151*, 111632. [CrossRef]

10. Farnham, C.; Yuan, J. Possible Perception Bias in the Thermal Evaluation of Evaporation Cooling with a Misting Fan. *Clean Technol.* **2021**, *3*, 183–205. [CrossRef]

11. Nada, S.; Fouda, A.; Mahmoud, M.; Elattar, H. Experimental investigation of energy and exergy performance of a direct evaporative cooler using a new pad type. *Energy Build.* **2019**, *203*, 109449. [CrossRef]

12. Fouda, A.; Melikyan, Z. A simplified model for analysis of heat and mass transfer in a direct evaporative cooler. *Appl. Therm. Eng.* **2011**, *31*, 932–936. [CrossRef]

13. Somwanshi, A.; Sarkar, N. Design and analysis of a hybrid air and water cooler. *Eng. Sci. Technol. Int. J.* **2019**, *23*, 101–113. [CrossRef]

14. Eidan, A.A.; Alwan, K.J.; AlSahlani, A.; Alfahham, M. Enhancement of the Performance Characteristics for Air-Conditioning System by Using Direct Evaporative Cooling in Hot Climates. *Energy Procedia* **2017**, *142*, 3998–4003. [CrossRef]

15. Atmaca, I.; Şenol, A.; Çağlar, A. Performance testing and optimization of a split-type air conditioner with evaporatively-cooled condenser. *Eng. Sci. Technol. Int. J.* **2021**, *32*, 101064. [CrossRef]

16. Afonicevs, V.; Strauts, U.; Bogdanovs, N.; Lesinskis, A. Evaporative cooling technology efficiency compared to traditional cooling system–case study. In Proceedings of the 19th International Scientific Conference Engineering for Rural Development, Jelgava, Latvia, 20−22 May 2020. [CrossRef]

17. Rashmi, S.; Nihar, S.; Amol, P. *Addressing Water Consumption of Evaporative Coolers with Greywater*; Lawrence Berkeley National Laboratory: Berkeley, CA, USA, 2012.

18. Bhatkar, V.W. Determination of water loss for an adiabatic cooling of a fin fan water cooler. *Mater. Today Proc.* **2021**, *47*, 5629–5631. [CrossRef]

19. Rafique, M.M.; Gandhidasan, P.; Rehman, S.; Al-Hadhrami, L.M. A review on desiccant based evaporative cooling systems. *Renew. Sustain. Energy Rev.* **2015**, *45*, 145–159. [CrossRef]

20. Yamada, H.; Yoon, G.; Okumiya, M.; Okuyama, H. Study of cooling system with water mist sprayers: Fundamental examination of particle size distribution and cooling effects. *Build. Simul.* **2008**, *1*, 214–222, In: IBPSA 2007-International Building Performance Simulation Association 2007. [CrossRef]

21. Khangembam, C.; Singh, D.; Handique, J.; Singh, K. Experimental and numerical study of air-water mist jet impingement cooling on a cylinder. *Int. J. Heat Mass Transf.* **2020**, *150*, 119368. [CrossRef]

22. Fawzy, H.; Zheng, Q.; Jiang, Y.; Lin, A.; Ahmad, N. Conjugate heat transfer of impingement cooling using conical nozzles with different schemes in a film-cooled blade leading-edge. *Appl. Therm. Eng.* **2020**, *177*, 115491. [CrossRef]

23. Sadafi, M.; Jahn, I.; Hooman, K. Nozzle arrangement effect on cooling performance of saline water spray cooling. *Appl. Therm. Eng.* **2016**, *105*, 1061–1066. [CrossRef]

24. Bao, J.; Wang, Y.; Xu, X.; Niu, X.; Liu, J.; Qiu, L. Analysis on the influences of atomization characteristics on heat transfer characteristics of spray cooling. *Sustain. Cities Soc.* **2019**, *51*, 101799. [CrossRef]

25. Sun, T.; Huang, X.; Chen, Y.; Zhang, H. Experimental investigation of water spraying in an indirect evaporative cooler from nozzle type and spray strategy perspectives. *Energy Build.* **2020**, *214*, 109871. [CrossRef]

26. Sajjad, U.; Abbas, N.; Hamid, K.; Abbas, S.; Hussain, I.; Ammar, S.M.; Sultan, M.; Ali, H.M.; Hussain, M.; Rehman, T.U.; et al. A review of recent advances in indirect evaporative cooling technology. *Int. Commun. Heat Mass Transf.* **2021**, *122*, 105140. [CrossRef]

27. De Antonellis, S.; Joppolo, C.M.; Liberati, P.; Milani, S.; Molinaroli, L. Experimental analysis of a cross flow indirect evaporative cooling system. *Energy Build.* **2016**, *121*, 130–138. [CrossRef]

28. Al-Zubaydi, A.Y.T.; Hong, G. Experimental study of a novel water-spraying configuration in indirect evaporative cooling. *Appl. Therm. Eng.* **2019**, *151*, 283–293. [CrossRef]

29. Borodinecs, A.; Lebedeva, K.; Prozuments, A.; Brahmanis, A.; Grekis, A.; Zajecs, D.; Zekunde, A.; Vatin, N. Feasibility of reducing electricity consumption of air conditioning equipment by condenser direct evaporative cooling technology. Example of case study in dubai. *Atmosphere* **2021**, *12*, 1205. [CrossRef]

30. Xu, P.; Ma, X.; Diallo, T.M.O.; Zhao, X.; Fancey, K.; Li, D.; Chen, H. Numerical investigation of the energy performance of a guideless irregular heat and mass exchanger with corrugated heat transfer surface for dew point cooling. *Energy* **2016**, *109*, 803–817. [CrossRef]

31. Duan, Z.; Zhan, C.; Zhao, X.; Dong, X. Experimental study of a counter-flow regenerative evaporative cooler. *Build. Environ.* **2016**, *104*, 47–58. [CrossRef]

32. Prozuments, A.; Brahmanis, A.; Mucenieks, A.; Jacnevs, V.; Zajecs, D. Preliminary Study of Various Cross-Sectional Metal Sheet Shapes in Adiabatic Evaporative Cooling Pads. *Energies* **2022**, *15*, 3875. [CrossRef]

33. Lee, K. *Principles of CAD/CAM/CAE Systems*; Pearson Education: London, UK, 1999.

34. Russell, S.; Norvig, P. *Artificial Intelligence: A Modern Approach*, 2nd ed.; Prentice Hall: Hoboken, NJ, USA, 2002.

35. Norenkov, I.P.; Kuzmik, P.K. *Information Support for High Technology Products (CALS technologies)*; Bauman Moscow State Technical University: Moscow, Russia, 2002; 320p, ISBN 5-7038-1962-8. (In Russian)

36. Kolchin, A.F.; Ovsyannikov, M.V.; Strekalov, A.F.; Sumarokov, S.V. Product Life Cycle Management. 2007, LLC "Anacharsis", Moscow (2002). Available online: https://context.reverso.net/translation/english-russian/product+life-cycle+management (accessed on 1 June 2022). (In Russian).

37. Alyamovsky, A.A.; Sobachkin, A.A.; Odintsov, E.V.; Kharitonovich, A.I.; Ponomarev, N.B. SolidWorks. Computer modeling in engineering practice. In Proceedings of the InMotion Project Final Conference, Saint Petersburg, Russia, 27–29 June 2005. (In Russian)
38. Petrila, T.; Trif, D. *Basics of Fluid Mechanics and Introduction to Computational Fluid Dynamics*; Springer: Berlin/Heidelberg, Germany, 2005. [CrossRef]
39. Wilcox, D.C. *Turbulence Modeling for CFD*; DCW Industries: La Canada, CA, USA, 1993.
40. Loytsyansky, L.G. Mechanics of Liquid and Gas. Master's Thesis, Samara University, Samara, Russia, 2003. (In Russian).
41. Janna, W.S. *Introduction to Fluid Mechanics, Fifth Edition*; Taylor Francis Group: Abingdon, UK, 2015. [CrossRef]
42. The 3DEXPERIENCE Company. Dassault Systèmes Provides Business and People with Virtual Universes to Imagine Sustainable Innovations Capable of Harmonizing Product, Nature and Life. Available online: https://www.3ds.com/ (accessed on 25 May 2022).
43. Pazhi, D.G.; Galustov, V.S. *Sprays of Liquid*; Khimiya: Moscow, Russia, 1979. (In Russian)
44. Pazhi, D.G.; Galustov, V.S. *Fundamentals of Spraying Technology*; Khimiya: Moscow, Russia, 1984. (In Russian)